Bulletin of the Earthquake
Research Institute
Vol. 55 (1980), pp. 27-41

2. *Pseudomagnetic Anomaly Derived from Gravity Observations in Central Japan.*

By Yukio Hagiwara,

Earthquake Research Institute University of Tokyo.

(Received February 25, 1980)

Abstract

A pseudomagnetic intensity anomaly is calculated from the Bouguer anomaly assuming both the anomalies to be generated by a common source structure. Applying the conversion formulas between gravity and magnetic anomalies to the observed gravity and aeromagnetic data, we find that central Japan consists of three zones, i.e. negative, positive and non-correlation zones between the observed and the calculated total-intensity anomalies. They extend northward from the Pacific side. It appears reasonable to suggest that the positive and the negative zones correspond to normal and reverse magnetizations respectively.

1. Introduction

Ishikawa (1979) has recently compiled the aeromagnetic data of central Japan obtained by the Geographical Survey Institute. He pointed out that the total-intensity magnetic anomaly over the northern part of the Fossa Magna area matches satisfactorily the short wavelength Bouguer anomaly presented by Hagiwara (1967). This coincidence may possibly imply that both gravity and magnetic anomalies are related to a common generating source. In such a case, the magnetic anomaly can be derived from the Bouguer anomaly and vice versa on the basis of the theory of potential field, assuming causative bodies with homogeneous magnetization and uniform density.

The proposal of a mathematical method connecting the magnetic potential with a gravity potential dates back to Baranov (1957). Robinson (1971) has provided a much simpler expression for a pseudo-total-intensity magnetic field extracted from a gravity field by using Poisson's relation, with its application to some idealized source models. This paper presents an approach to the gravity-magnetic field transformation method using the Fourier integral transform in the frequency domain. The transformation formulas from gravity to magnetic anomaly components are expressed in simple convolution integrals

and converted into digital forms convenient for actual computations.

Furthermore, the practical application of these formulas are made on gravity and aeromagnetic data observed in central Japan. As far as the author knows, there are very few articles dealing with actual data, although many descriptions of the transformation methods and model calculations have already been published. If the pseudomagnetic field calculated from the Bouguer anomaly is similar to the aeromagnetic field, the source structure is presumed as common. If the magnetic field is involved in terrain effects, the observed magnetic anomaly may have a correlation with the pseudomagnetic one calculated from a free-air anomaly, because it depends largely on station elevation in contrast to the Bouguer anomaly independent of terrain effects. A magnetization in reverse to the earth's present magnetic field can be expected as a negative correlation. The correlation coefficient consideration, in this sense, might from a geomagnetic viewpoint be the key to the problem of zoning buried geological structures.

2. Method of Analysis

2-1. Relationship between Gravity and Magnetic Fields.

The gravity potential U at a point P (x, y, z) due to an anomalous body v with the density contrast $\Delta\rho$ has the expression

$$U=G\Delta\rho\iiint_v \frac{dv}{r} \tag{1}$$

where G is Newton's gravitational constant and r the distance between the attracted point P and a mass element $\Delta\rho\, dv$. For simplicity, $\Delta\rho$ is assumed to be constant.

On the other hand, the magnetic potential is written as

$$V=J\iiint_v \operatorname{grad}\left(\frac{1}{r}\right) dv \tag{2}$$

where J is the magnetization vector assuming that the direction and magnitude of J are the same in all magnetized bodies.

Combination of (1) and (2) gives a relation

$$V=\frac{J}{G\Delta\rho}\operatorname{grad} U=\frac{J}{G\Delta\rho}\left(\alpha\frac{\partial U}{\partial x}+\beta\frac{\partial U}{\partial y}+\gamma\frac{\partial U}{\partial z}\right) \tag{3}$$

where $J=|J|$, and α, β and γ are direction cosines of J. This equation indicates that the magnetic potential can be calculated from the gravity potential. It should be noted here that, according to the convention of geomagnetism, the directions of x, y and z are taken

northward, eastward and downward, respectively. Denoting the declination and the dip angle of J by D and I respectively, we have

$$\left.\begin{aligned}\alpha&=\cos I\cos D\\ \beta&=\cos I\sin D\\ \gamma&=\sin I\end{aligned}\right\} \tag{4}$$

Note that $\alpha^2+\beta^2+\gamma^2=1$.

Taking derivatives of V with respect to x, y and z, the components of the magnetic anomaly ΔX, ΔY and ΔZ are derived as follows

$$\begin{pmatrix}\Delta X\\ \Delta Y\\ \Delta Z\end{pmatrix}=\frac{J}{G\Delta\rho}\begin{pmatrix}\frac{\partial^2U}{\partial x^2} & \frac{\partial^2U}{\partial x\partial y} & \frac{\partial^2U}{\partial x\partial z}\\ \frac{\partial^2U}{\partial x\partial y} & \frac{\partial^2U}{\partial y^2} & \frac{\partial^2U}{\partial y\partial z}\\ \frac{\partial^2U}{\partial x\partial z} & \frac{\partial^2U}{\partial y\partial z} & \frac{\partial^2U}{\partial z^2}\end{pmatrix}\begin{pmatrix}\alpha\\ \beta\\ \gamma\end{pmatrix} \tag{5}$$

The corresponding total-intensity magnetic anomaly can then be approximated as

$$\Delta F\simeq\alpha\Delta X+\beta\Delta Y+\gamma\Delta Z \tag{6}$$

in which second and higher order terms of increments are neglected.

In most cases, the frequency domain representation of a formula is very useful for solving problems of the potential theory in the Cartesian rectangular coordinates. The Fourier integral transform is a powerful tool applicable to the present study. Both sides of (5) are transformed into a frequency domain, and after some algebra (see Appendix) we take the inverse transform to obtain the following expressions

$$\begin{pmatrix}\Delta X(x,\,y,\,-H)\\ \Delta Y(x,\,y,\,-H)\\ \Delta Z(x,\,y,\,-H)\\ \Delta F(x,\,y,\,-H)\end{pmatrix}=\frac{J}{2\pi G\Delta\rho}\iint_{-\infty}^{\infty}\begin{pmatrix}\psi_x(x-x',\,y-y',\,-H)\\ \psi_y(x-x',\,y-y',\,-H)\\ \psi_z(x-x',\,y-y',\,-H)\\ \psi(x-x',\,y-y',\,-H)\end{pmatrix}\Delta g(x',\,y',\,0)\,dx'dy' \tag{7}$$

where $z=-H$ is an altitude at which aeromagnetic surveys are conducted, Δg is the gravity anomaly distribution at an altitude of $z=0$, and the kernel functions are given as

$$\begin{pmatrix}\psi_x(x, y, -H)\\ \psi_y(x, y, -H)\\ \psi_z(x, y, -H)\\ \psi(x, y, -H)\end{pmatrix}=\frac{1}{(x^2+y^2+H^2)^{3/2}}\left\{\frac{3(\alpha x+\beta y+\gamma H)}{x^2+y^2+H^2}\begin{pmatrix}x\\ y\\ H\\ \alpha x+\beta y+\gamma H\end{pmatrix}-\begin{pmatrix}\alpha\\ \beta\\ \gamma\\ 1\end{pmatrix}\right\} \tag{8}$$

It is clear that

$$\psi=\alpha\psi_x+\beta\psi_y+\gamma\psi_z \tag{9}$$

is satisfied in the first-order approximation theory on the analogy of (6).

2-2. Digitalizing for Actual Computations

Since the kernel functions are given, the three components and total-intensity anomaly can be calculated by numerically integrating (7) from known gravity anomaly data. In this case, using a rectangular grid whose spacings are s_1 and s_2 along the x and y axes, respectively, the integrals of (7) are converted into digital forms

$$\begin{pmatrix}\Delta X(m, n, -\delta)\\ \Delta Y(m, n, -\delta)\\ \Delta Z(m, n, -\delta)\\ \Delta F(m, n, -\delta)\end{pmatrix}=\frac{J}{2\pi G\Delta\rho}\sum_{m'=-M}^{M}\sum_{n'=-N}^{N}\begin{pmatrix}\bar{\psi}_x(m-m', n-n', -\delta)\\ \bar{\psi}_y(m-m', n-n', -\delta)\\ \bar{\psi}_z(m-m', n-n', -\delta)\\ \bar{\psi}(m-m', n-n', -\delta)\end{pmatrix}\overline{\Delta g}(m', n', 0) \tag{10}$$

with integer numbers m and n indicating x and y coorninates, i.e. $m=x/s_1$ and $n=y/s_2$, and $\delta=H/s_1$. The limits of the summations M and N depend on δ. M and N are chosen to be 4 in this study because δ is smaller than 0.5 as will be mentioned in the forthcoming section. $\overline{\Delta g}$ is the block mean gravity anomaly in an area of $s_1\times s_2$, and

$$\left.\begin{aligned}\psi_x(m, n, -\delta)&=\int_{(m-1/2)s_1}^{(m+1/2)s_1}\mathrm{d}x\int_{(n-1/2)s_2}^{(n+1/2)s_2}\psi_x(x, y, -H)\,\mathrm{d}y\\ &=\alpha I_1(m, n, -\delta)+\beta I_2(m, n, -\delta)+\gamma I_3(n, m, -\delta)\\ \psi_y(m, n, -\delta)&=\alpha I_2(m, n, -\delta)+\beta I_1(n, m, -\delta)+\gamma I_3(m, n, -\delta)\\ \psi_z(m, n, -\delta)&=\alpha I_3(n, m, -\delta)+\beta I_3(m, n, -\delta)\\ &\quad-\gamma\{I_1(m, n, -\delta)+I_1(n, m, -\delta)\}\end{aligned}\right\} \tag{11}$$

$$\left.\begin{aligned}\psi(m, n, -\delta)=&\alpha^2 I_1(m, n, -\delta)+\beta^2 I_1(n, m, -\delta)\\&-\gamma^2\{I_1(m, n, -\delta)+I_1(n, m, -\delta)\}\\&+2\alpha\beta I_2(m, n, -\delta)+2\beta\gamma I_3(m, n, -\delta)\\&+2\gamma\alpha I_3(n, m, -\delta)\end{aligned}\right\}$$

where

$$\left.\begin{aligned}I_1(m, n, -\delta)&=-\left\|\frac{xy}{(x^2+H^2)\sqrt{x^2+y^2+H^2}}\right|_{x=(m-1/2)s_1}^{x=(m+1/2)s_1}\Bigg|_{y=(n-1/2)s_2}^{y=(n+1/2)s_2}\\I_2(m, n, -\delta)&=\left\|\frac{1}{H}-\frac{1}{\sqrt{x^2+H^2}}-\frac{1}{\sqrt{y^2+H^2}}\right.\\&\qquad\left.+\frac{1}{\sqrt{x^2+y^2+H^2}}\right|_{x=(m-1/2)s_1}^{x=(m+1/2)s_1}\Bigg|_{y=(n-1/2)s_2}^{y=(n+1/2)s_2}\\I_3(m, n, -\delta)&=\left\|\frac{x}{H\sqrt{x^2+H^2}}-\frac{xH}{(y^2+H^2)\sqrt{x^2+y^2+H^2}}\right|_{x=(m-1/2)s_1}^{x=(m+1/2)s_1}\Bigg|_{y=(n-1/2)s_2}^{y=(n+1/2)s_2}\end{aligned}\right\}\qquad(12)$$

3. Data and Computation Results

3-1. Gravity Data

A nationwide gravity survey was made at about 12,000 stations by the Geographical Survey Institute along the first- and second-order leveling routes. The routes sometimes cross over the backbone mountain range of the Japan island-arc, so that the terrain effect on gravity can not be neglected in determining the Bouguer anomaly. HAGIWARA (1967) completed terrain correction on the above gravity data and found the correction value to be in excess of 20 mgals in the central part of Japan proper.

The free-air anomaly varies so markedly with station elevation that the free-air map has a strong resemblance to the topographic map. On the contrary, the Bouguer anomaly is rather independent of topography. HAGIWARA (1967) drew a free-air anomaly map by subtracting Bouguer corrections from the terrain-corrected Bouguer anomaly map at grid points.

Figs. 1 and 2 show the terrain-corrected Bouguer anomaly and thus obtained free-air anomaly maps of the central part of Japan, which are available for calculating magnetic anomalies in the present study. As seen in Fig. 1, the negative Bouguer anomaly covers this area extensively with a roughly negative correlation to the topographical elevation. We also see that a narrow and deep negative anomaly

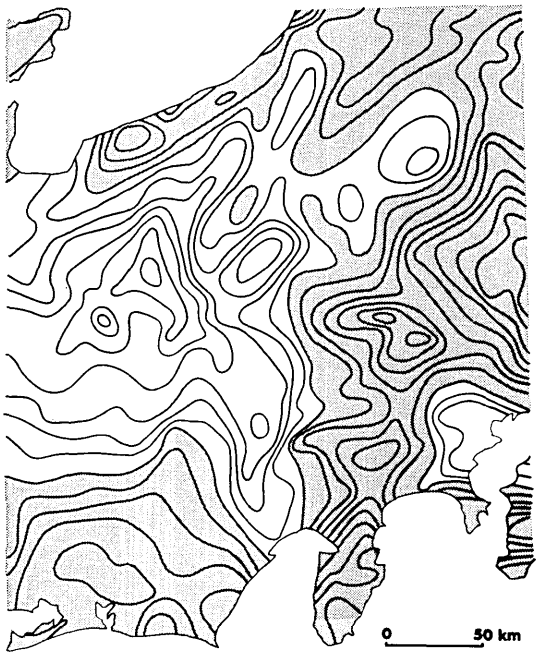

Fig. 1. Terrain-corrected Bouguer anomaly map of the central part of Japan. Stippled area indicates a positive anomaly. Contour interval is 10 mgal.

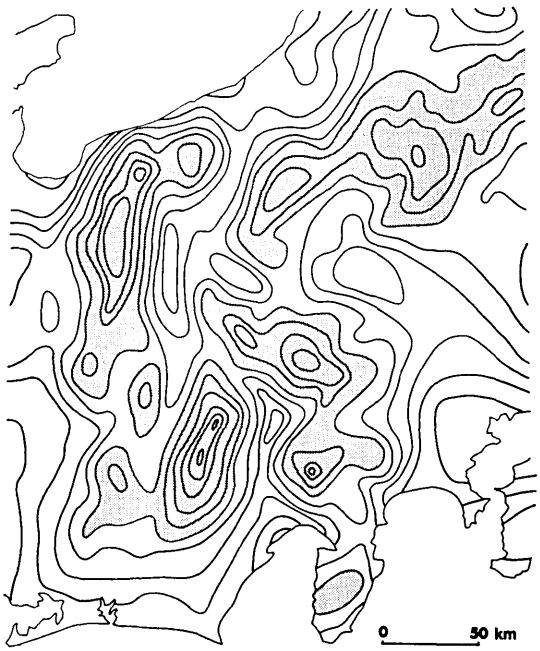

Fig. 2. Free-air anomaly map of the central part of Japan. Stippled area indicates a positive anomaly larger than 100 mgal. Contour interval is 20 mgal.

zone coincides with the Itoigawa-Shizuoka Geotectonic Line on the western border of the Fossa Magna area.

3-2. Magnetic Data

The magnetic data has been obtained by the Geographical Survey Institute along north-south flight lines 10 km apart and 3 km above sea level in 1965, 1967 and 1976. The 1977 aeromagnetic survey was conducted along east-west flight lines. ISHIKAWA (1979) made interpolations by using the cubic spline method (BHATTACHARYYA, 1969) for compiling the magnetic data in an area of 137° to 139°40'E by 34°24' to 37°24'N. Fig. 3 shows the total-intensity map thus obtained. The stippled areas on this map represent positive anomalies. Furthermore, he derived three components of magnetic anomaly from the

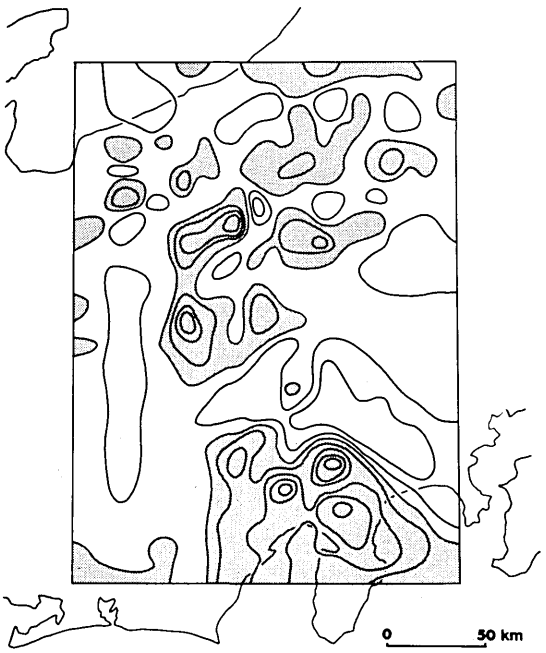

Fig. 3. Total-intensity aeromagnetic anomaly map with a contour interval of 100 nT obtained at an altitude of 3 km above sea level by the Geographical Survey Institute and compiled by ISHIKAWA (1979). Stippled area represents a positive anomaly.

total-intensity anomaly according to the method introduced by LOURENCO and MORRISON (1973).

The dominant feature of the total-intensity map is an extensive negative anomaly covering the northern half of the mapped area, in contrast to a conspicuous positive zone in the southern part. This

contrast may be caused by differences in geological features between the north and the south Fossa Magna regions. The northern negative anomaly is, as seen in the figure, dotted with intermediate-sized positive anomalies, one of which is located over the "central belt of uplift" characterized by a continuous crustal uplift. ISHIKAWA (1979) pointed out that this positive anomaly also corresponds to the positive zone of the short-wavelength Bouguer anomaly, in which the anomaly of wavelength longer than 160 km is eliminated.

Small highs isolated in the southern positive zone are apparently associated with volcanoes, such as Fuji, Hakone and Izu-oshima. These highs are not always correlated with the short-wavelength Bouguer highs. This may indicate the fact that strong magnetized materials with small densities cover or intrude into the volcanic bodies.

3-3. Pseudototal Magnetic Field Intensity Anomaly

We calculate pseudototal-intensity anomaly distribution at the 3 km elevation of the aeromagnetic survey from block mean data of the Bouguer anomaly. The spacings of grid used are 4′ latitude and 6′ longitude, i.e. roughly $s_1 \fallingdotseq 7.4$ km and $s_2 \fallingdotseq 9.0$ km, respectively. The summations with respect to m' and n' are truncated at $M=N=4$, as

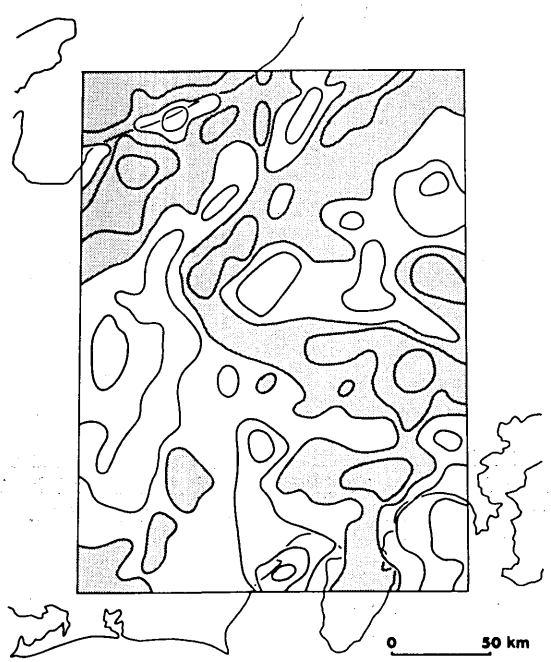

Fig. 4. Pseudototal-intensity anomaly map with a contour interval of 100 nT calculated at the 3 km elevation of the aeromagnetic survey. Stippled area represents a positive anomaly.

the truncation error becomes small when we take $\delta = 3/7.4 \fallingdotseq 0.4$. The mean dip and declination angles in the central part of Japan are adopted, and the ratio of magnetization coefficient to density contrast is taken as $J/(2\pi G \Delta\rho) = 2 \times 10^4$ emu sec^2/cm^3 for our calculation.

The pseudototal-intensity map thus calculated is shown in Fig. 4. It is apparent that the pattern of the northeast-trending positive anomaly zone (stippled area) in the northern part of this map has a strong resemblance to that of Fig. 3. This zone coincides with the central belt of uplift. Likewise, in the western margins of both the maps, we can see elongated north-south trending negative anomalies, indicated by -100 nT contours, over the valley systems along Matsumoto and Ina basins.

On the other hand, the anomaly patterns are quite different from each other at the southeastern corner of the mapped area, where some isolated positive anomalies are located over volcanoes. According to the current theory of plate tectonics, this area is characterized by a collision of the Philippine Sea plate with the continental lithosphere. Continuous earthquake activities take place there by wedging the tip of the oceanic plate into the central Japan crust. From this point of view, we expect another type of similitude between observed magnetic anomaly patterns and those calculated from gravity data.

3-4. Geomagnetic Zoning

To compare the detailed configuration on both the maps, three cross sections are illustrated in Fig. 5. Cross section a-a′ intersects the positive anomaly zone on the central belt of uplift. The correlation between the observed anomalies (solid line) and the calculated ones (dotted line) is apparently well established, although the amplitude of the calculated anomaly is generally less than that of the observed one. The problem of such a difference in amplitude can be solved by adjusting the ratio of $J/(2\pi G \Delta\rho)$. The fact that both the profiles resemble each other can indicate the normal magnetization of the source structure along the cross section.

On the magnetic profiles along cross section b-b′, we find two inversely correlated local areas, i.e. one of peaks of the observed anomaly profile coincides with a minimum pseudototal-intensity and vice versa. Such an inverse correlation might possibly be caused by a source body magnetized reversely to the earth's present magnetic field, but we have no rock-magnetism data available to be accepted as sufficient evidence for the reverse magnetization in these two areas. Cross section c-c′ indicates north-south profiles. The south end of this section is occupid by an inversely correlated area.

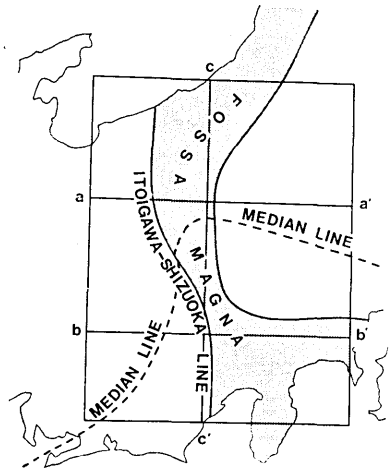

Fig. 5-1.

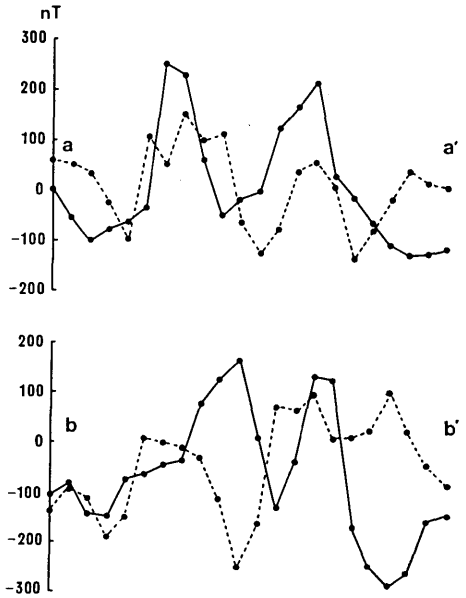

Fig. 5-2.

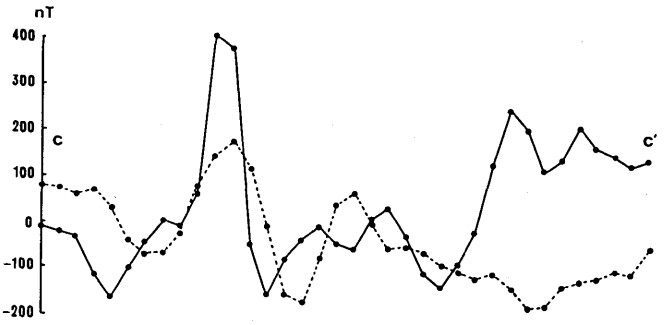

Fig. 5-3.

Fig. 5. Profiles of observed tatal-intensity anomalies (solid line) and those calculated (dotted line) along cross sections a-a', b-b' and c-c'.

It is interesting to see the regional distribution of the correlation between observed and calculated total-intensity anomalies. The stippled areas in Fig. 6 represent squares of grid where both the anomalies are positive or negative. In the remaining areas, the anomalies take signs different from each other. Thick lines draw boundaries between Zones A, B and C from the Pacific side to the Japan Sea coast. The stippled squares cluster in Zone B, while the open squares are mainly distributed in Zones A and C.

Zone A consisting of 260 squares of grid has a negative correlation coefficient of -0.25 between the aeromagnetic anomaly and the one calculated from the Bouguer anomaly. This amount of coefficient is

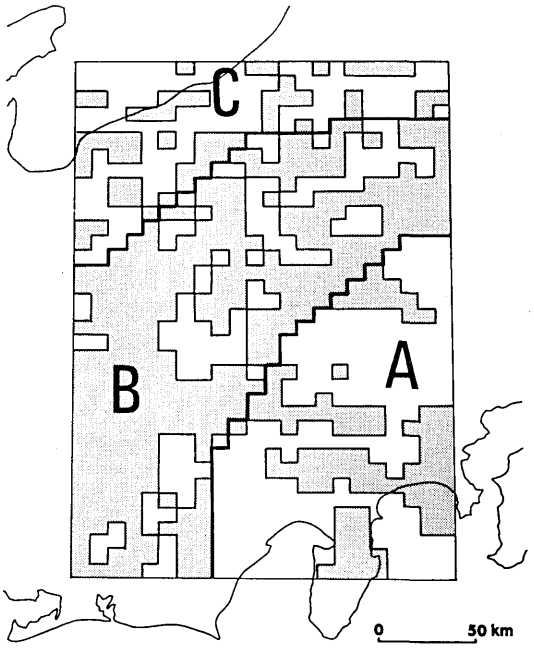

Fig. 6. Regional distribution of correlation between observed total-intensity anomalies and those calculated. Stippled areas represent squares of grid where both the anomalies are positive or negative.

Table 1. Correlation coefficients between observed total-intensity anomalies and those calculated from gravity anomalies.

	Zone	Pseudototal-intensity anomalies calculated from	
		Bouguer anomaly	free-air anomaly
Total-intensity aeromagnetic anomaly	A	−0.25	0.09
	B	0.36	−0.08
	C	−0.04	0.13

statistically significant for verifying the hypothesis that both the anomalies are inversely correlated in Zone A. Zone B consisting of 375 samples has a positive correlation coefficient amounting to 0.36, which is confirmed by a significant test. However, the statistical consideration of Zone C results in almost no correlation. The correlation coefficients are given in Table 1.

Correlation coefficients between observed total-intensity anomaly and those calculated from free-air gravity anomaly are also considered in order to check terrain effects on the magnetic field. The free-air anomaly depends largely on terrain effects, so that the correlation

coefficient between observed magnetic amomaly and that calculated from free-air anomaly is a good indicator of terrain effects. The results of the pseudomagnetic calculation from free-air gravity anomaly are also added to Table 1. Apparently, the aeromagnetic data is scarcely related to topographic relief throughout the region concerned.

4. Conclusion

The sophisticated mathematical procedures using Fourier integral transforms describe the relationship between total-intensity anomaly of the aeromagnetic field and pseudototal-intensity anomaly calculated from gravity data. The practical application of this method is made to the gravity and aeromagnetic data observed in the central part of Japan. Comparison between observed total-intensity anomaly and that calculated from the Bouguer anomaly gives zoning A, B and C from the Pacific side to the Japan Sea coast. As given in Table 1, these three zones correspond respectively to negative, positive and almost

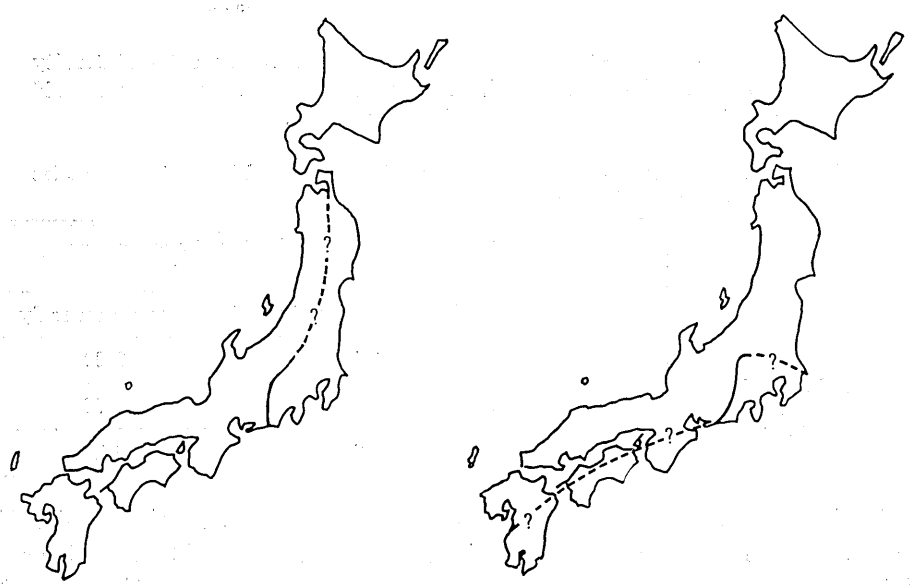

Fig. 7. Further extension of the A–B boundary line to be expected. a) Northward extension along the island-arc. b) Westward extension along the Median Geotectonic Line.

zero correlation coefficients between the aeromagnetic and the pseudomagnetic anomalies. The positive correlation is presumed as common source structures for both gravity and magnetic anomaly fields, and the negative correlation might possibly be inferred to be caused by

the reverse magnetization.

Our special interest is in the further extension of these three zones. One of the possibilities is that the zonal arrangement extends northwards along the Japan island-arc. In this case, a similar zone structure will be found in northeast Japan. Unfortunately, the aeromagnetic survey results there have not been compiled yet by the Geographical Survey Institute, so that the aeromagnetic data are not available for the present study. On the other hand, the westward extension of the zonal arrangement along the Median Geotectonic Line can be expected. The pseudototal-intensity analyses of the Bouguer anomaly over the Kii peninsula, Shikoku and Kyushu islands can reveal the zonal geological structure in comparison with the aeromagnetic data. The Geographical Survey Institute is planning to survey these districts in the near future. If the aeromagnetic survey is completed in these remaining districts, aero- and psudomagnetic comparison as presented in this paper should give useful information to the geological investigations of Japan's island-arc structure.

Appendix

The Fourier integral transform of $U(x, y, z)$ with respect to x and y is denoted by

$$U^*(\omega_1, \omega_2, z) = \iint_{-\infty}^{\infty} U(x, y, z) \exp\{-i(\omega_1 x + \omega_2 y)\}\, dx\, dy \qquad \text{(A-1)}$$

where ω_1 and ω_2 are the angular frequencies having a dimension of reciprocal length, and $i=\sqrt{-1}$. By definition, the asterisk denotes the Fourier transform throughout this paper. The inverse transform of (A-1) is given by

$$U(x, y, z) = \frac{1}{4\pi^2} \iint_{-\infty}^{\infty} U^*(\omega_1, \omega_2, z) \exp\{i(\omega_1 x + \omega_2 y)\}\, d\omega_1\, d\omega_2 \qquad \text{(A-2)}$$

We take the Fourier transforms of both sides of (5), obtaining

$$\begin{pmatrix} \Delta X^* \\ \Delta Y^* \\ \Delta Z^* \end{pmatrix} = -\frac{J}{G\Delta\rho} \begin{pmatrix} \omega_1 \\ \omega_2 \\ i\dfrac{\mathrm{d}}{\mathrm{d}z} \end{pmatrix} \left\{ (\alpha\omega_1 + \beta\omega_2) U^* + i\gamma \frac{\mathrm{d}U^*}{\mathrm{d}z} \right\} \qquad \text{(A-3)}$$

In order to eliminate derivatives of U^* with respect to z from (A-3), we consider the well-known Laplace differential equation satisfying in a space outside the mass distribution, that is

$$\frac{\partial^2 U}{\partial x^2}+\frac{\partial^2 U}{\partial y^2}+\frac{\partial^2 U}{\partial z^2}=0 \tag{A-4}$$

The Fourier transform of (A-4) is described as

$$\frac{\mathrm{d}^2 U^*}{\mathrm{d}z^2}-\omega^2 U^*=0$$

the solution of which is

$$U^*(\omega_1, \omega_2, z)=U^*(\omega_1, \omega_2, 0)e^{\omega z} \tag{A-5}$$

where $\omega^2=\omega_1^2+\omega_2^2$.

Since the gravity potential is not directly observable, the gravity anomaly Δg is used for our present purpose instead of U. The Fourier transform of the gravity anomaly at sea level $z=0$ becomes

$$\Delta g^*(\omega_1, \omega_2, 0)=\left[\frac{\mathrm{d}U^*}{\mathrm{d}z}\right]_{z=0} =\omega U^*(\omega_1, \omega_2, 0)$$

Therefore

$$U^*(\omega_1, \omega_2, z)=\frac{e^{\omega z}}{\omega}\Delta g^*(\omega_1, \omega_2, 0) \tag{A-6}$$

Then we rewrite (A-3) as follows

$$\begin{pmatrix} \Delta X^*(\omega_1, \omega_2, -H) \\ \Delta Y^*(\omega_1, \omega_2, -H) \\ \Delta Z^*(\omega_1, \omega_2, -H) \end{pmatrix}=-\frac{J}{G\Delta\rho}\begin{pmatrix} \omega_1/\omega \\ \omega_2/\omega \\ i \end{pmatrix}(\alpha\omega_1+\beta\omega_2+i\gamma\omega)e^{-\omega H}\Delta g^*(\omega_1, \omega_2, 0) \tag{A-7}$$

The total-intensity anomaly is transformed into

$$\Delta F^*(\omega_1, \omega_2, -H)=-\frac{J}{G\Delta\rho}\frac{(\alpha\omega_1+\beta\omega_2+i\gamma\omega)^2}{\omega}e^{-\omega H}\Delta g^*(\omega_1, \omega_2, 0) \tag{A-8}$$

Our problem is to obtain the space domain representations of (A-7) and (A-8), which can be easily obtained by the inverse Fourier transforms as in (7). In this case, the kernel function ψ_x is calculated from

$$\psi_x(x, y, -H)=-\frac{1}{2\pi}\iint_{-\infty}^{\infty}\frac{\omega_1}{\omega}(\alpha\omega_1+\beta\omega_2+i\gamma\omega)e^{-\omega H}\exp\{i(\omega_1 x+\omega_2 y)\}\mathrm{d}\omega_1\mathrm{d}\omega_2$$

$$=\frac{1}{(x^2+y^2+H^2)^{3/2}}\left\{\frac{3x(\alpha x+\beta y+\gamma H)}{x^2+y^2+H^2}-\alpha\right\}$$

Similarly to the above, we can prove that the other kernel functions become (8).

References

BARANOV, V., 1957, A new method for interpretation of aeromagnetic maps: pseudogravimetric anomalies, *Geophysics*, **22**, 359-383.

BHATTACHARYYA, B. K., 1969, Bicubic spline interpolation as a method for treatment of potential field data, *Geophysics*, **34**, 402-423.

HAGIWARA, Y., 1964, Analyses of gravity values in Japan, *Bull. Earthq. Res. Inst., Univ. Tokyo*, **45**, 1091-1228.

ISHIKAWA, Y., 1979, The magnetic anomaly in the central part of Japan derived from the aeromagnetic survey results (in Japanese), Thesis of M. Sc. submitted to the University of Tokyo.

LOURENCO, J. S. and MORRISON, H. F., 1973, Vector magnetic anomalies derived from measurements of a single component of the field, *Geophysics*, **38**, 359-368.

RORINSON, E. S., 1971, The use of Poisson's relation for the extraction of pseudototal magnetic field intensity from gravity observations, *Geophysics*, **36**, 605-608.

---

2. 中部日本の重力データから導かれた疑似全磁力異常

地震研究所　萩　原　幸　男

重力と地磁気の異常が同一の構造を反映していると仮定して，ブーゲー異常から導いた全磁力異常を疑似全磁力異常という．本論文では，まずブーゲー異常と疑似全磁力異常との関係をフーリエ積分によって表わし，ついでこの関係式を用いて，中部日本のブーゲー異常から疑似全磁力異常を計算し，それを石川 (1979) がコンパイルした全磁力異常と比較する．

比較の結果，両全磁力異常の相関から，中部日本は太平洋側より，A, B, C の3地域に分けられることがわかった．A は両全磁力異常が負の相関をもつ地域，B は正の相関，C はほとんど無相関の地域である．負の相関は地球磁場の反転に関係するとも思われ興味深い．またこれら3地域が，帯状に東北日本列島弧に延びるものか，あるいは中央構造線に沿って西南日本列島弧にその延長が見出せるか，これまた興味深い問題である．